Climate Dynamics (2023) 60:47–63
https://doi.org/10.1007/s00382-022-06300-6

Relative contributions to ENSO of the seasonal footprinting and trade wind charging mechanisms associated with the Victoria mode

Kai Ji[1] · Yuheng Tseng[2] · Ruiqiang Ding[3,4] · Jiangyu Mao[4] · Licheng Feng[5,6]

Received: 16 September 2021 / Accepted: 13 April 2022 / Published online: 6 May 2022

Abstract

The Victoria mode (VM), as a basin-scale sea surface temperature (SST) pattern over the North Pacific, is suggested to facilitate subsequent development of El Niño–Southern Oscillation (ENSO) through both the seasonal footprinting mechanism (SFM) and the trade wind charging (TWC) mechanism. The present study aims at investigating the distinct roles and relative contributions to ENSO of the SFM and the TWC mechanism associated with the VM using atmospheric and oceanic reanalysis data as well as modeling simulations. Our results reveal that the positive SST anomalies (SSTAs) over the subtropical northeast Pacific (SNP) related to the VM effectively trigger the initiation of ENSO via the SFM, which emphasizes an air–sea surface thermodynamic-coupling process. In contrast, the negative SSTAs over the western North Pacific (WNP) associated with the VM primarily induce ENSO via a thermocline–SST feedback process, known as the TWC mechanism. Further analysis indicates that the SFM related to the VM may play a relatively independent role in affecting ENSO and is more closely linked to ENSO than is the TWC mechanism related to the VM, which is shown to be reasonably reproduced by the Community Earth System Model. Additionally, the SFM associated with the positive (negative) SNP SSTAs may induce fewer El Niño events (more La Niña events) than the TWC mechanism related to the positive (negative) WNP SSTAs. Our findings suggest that the SFM and the TWC mechanism associated with the VM both contribute to enhanced predictive skill for ENSO.

Keywords ENSO · Victoria mode · North Pacific SST · Air–sea interaction

1 Introduction

El Niño–Southern Oscillation (ENSO), characterized by sea surface temperature anomalies (SSTAs) in the eastern-to-central equatorial Pacific, is the strongest signal of interannual climate variability in the tropical Pacific. ENSO plays a vital role in global weather and climate anomalies (Wang et al. 2000; Alexander et al. 2002; Ashok et al. 2007; Wu and Zhang 2015; Dou et al. 2017; Zhang et al. 2017, 2018, 2019; Yu et al. 2018). The occurrence of extreme weather and climate events, such as droughts and surplus rainfall, is often affected by changes in the ENSO phase (Wang et al. 2000; Schubert et al. 2008; Grimm and Tedeschi 2009). Therefore, the dynamics, diversity, prediction, and impacts of the ENSO phenomenon have been extensively studied (Ashok et al. 2007; Kao and Yu 2009; Kug et al. 2009; Paek et al. 2017; Santoso et al. 2017, 2019).

Previous work has shown that a North Pacific Oscillation (NPO)-like extratropical atmospheric variability can trigger the occurrence of ENSO events (Linkin and Nigam 2008).

✉ Licheng Feng
fenglich@nmefc.cn

1 School of Environmental Studies, China University of Geosciences, Wuhan 430074, China

2 Institute of Oceanography, National Taiwan University, Taipei, Taiwan

3 State Key Laboratory of Earth Surface Processes and Resource Ecology, Beijing Normal University, Beijing 100875, China

4 State Key Laboratory of Numerical Modeling for Atmospheric Sciences and Geophysical Fluid Dynamics (LASG), Institute of Atmospheric Physics, Chinese Academy of Sciences, Beijing 100029, China

5 National Marine Environmental Forecasting Center, Ministry of Natural Resources, Beijing 100081, China

6 Key Laboratory of Marine Hazards Forecasting, National Marine Environmental Forecasting Center, Ministry of Natural Resources, Beijing 100081, China

Several mechanisms have been presented to explain the connection between the NPO and ENSO (e.g., Vimont et al. 2001, 2003a; Vimont et al. 2003b; Anderson 2003, 2004; Chang et al. 2007; Yu and Kim 2010; Wang et al.2012; Ding et al. 2015b). Recent studies have reported an NPO-induced sea surface temperature (SST) footprint in the North Pacific, referred to as the Victoria mode (VM), which exists over the whole extratropical North Pacific basin, including local-scale positive SSTAs over the subtropical northeast Pacific (SNP) and negative SSTAs over the western North Pacific (WNP).

The VM forced by the NPO effectively influences ENSO through both the seasonal footprinting mechanism (SFM) and the trade wind charging (TWC) mechanism (Ding et al. 2015a, b, 2018). In particular, the SFM shown in Vimont et al. (2003b) suggests that the NPO can reduce surface evaporation and increase SST in the SNP by reducing the speed of the subtropical northeasterly trade winds, leading to the formation of the Pacific Meridional Mode (PMM) in the SNP during the boreal spring. The PMM extends positive SSTAs southwestwards to the central equatorial Pacific via a wind–evaporation–SST (WES) feedback (Xie and Philander 1994; Chang et al. 2007), which favors the development of positive SSTAs in the central eastern equatorial Pacific. The SFM suggests that the NPO can ultimately lead to ENSO in the following winter through the above thermodynamic air–sea surface coupling processes. In contrast, the TWC hypothesis states that variations in North Pacific trade winds induced by the NPO can directly force subsurface heat content anomalies over the central equatorial Pacific, which are conducive to the occurrence of El Niño events (Anderson 2004; Anderson and Maloney 2006; Anderson et al. 2013b). Therefore, the TWC hypothesis primarily involves an ocean-dynamics process. In addition, the SSTAs in the western North Pacific (WNP) are proposed to act as a crucial precursor for ENSO (Wang et al 2012). The WNP-associated SST and wind anomalies contribute directly to oceanic Kelvin wave activity in the western tropical Pacific, causing the change in thermocline depth in the basin equatorial Pacific, which may effectively alter the subsurface temperature anomalies. Thus, the WNP is a key region that determines the ocean-dynamics process prior to ENSO events. Therefore, these mechanisms are considered to be the crucial initiator of ENSO events (Chakravorty et al. 2021). Nevertheless, the relative contributions of these mechanisms in triggering ENSO remain unclear.

In this study, we attempt to elucidate the relative contributions of the SFM and TWC mechanism associated with the VM in triggering ENSO by comprehensively analyzing reanalysis data and large-ensemble coupled model outputs. Given that the SSTAs over the SNP and the WNP effectively trigger the initiation of ENSO via the SFM and the TWC mechanism, respectively, we use the SNP and WNP SSTAs to represent the respective role of SFM and TWC associated with the VM. The aim is to further improve our understanding of the influence of the North Pacific SST variability on ENSO and thus aid the predictability of ENSO. The remainder of the paper is organized as follows: The observational data, numerical models, and methods used in this study are briefly introduced in Sect. 2. Section 3 reveals the different roles and relative contributions of the SFM and TWC mechanism associated with the VM in triggering the initiation of ENSO. Finally, Sect. 4 provides a discussion and conclusions.

2 Data and methods

2.1 Data

The monthly SST data used in this study are from the Hadley Centre Global Sea Ice and Sea Surface Temperature dataset, version 1.1 (Rayner et al. 2003), on a global $1° \times 1°$ longitude–latitude grid, and were obtained from the website of the Met Office Hadley Centre (https://www.metoffice.gov.uk/hadobs/hadisst/data/download.html). The subsurface ocean temperature data originate from the Institute of Atmospheric Physics' ocean gridded products, which have a horizontal resolution of $1° \times 1°$ (Cheng et al. 2017). This dataset has 41 vertical levels distributed from 1 to 2000 m for the period 1950–2017. For atmospheric variables, we use the monthly fields of sea level pressure (SLP) and surface wind from the National Centers for Environmental Prediction–National Center for Atmospheric Research Reanalysis 1 dataset on a $2.5° \times 2.5°$ latitude–longitude grid (Kalnay et al. 1996) for the period 1950–2017. Monthly anomalies were calculated by removing climatological means for each month. All data used in this study are linearly detrended prior to calculation. To better isolate the interannual linkage, we extract high-frequency variability of all datasets by using a 13-year high-pass Fourier filter.

To examine the difference between the relative independent contributions to ENSO of the SNP-SSTA and WNP-SSTA patterns associated with the VM, we employ the output of the first 30 members of the Community Earth System Model Large Ensemble Community Project (CESM-LENS) forced with historical radiative fluxes from 1950 to 2005, which is available at https://www.cesm.ucar.edu/projects/community-projects/LENS/data-sets.html (Kay et al. 2015).

2.2 Index definitions

Following Ding et al. (2015b), the empirical orthogonal function (EOF) analysis of the monthly SSTA field for the period 1950–2017 was performed in this study over the North Pacific (20°–66° N, 124°E–99° W; Fig. 1). The first

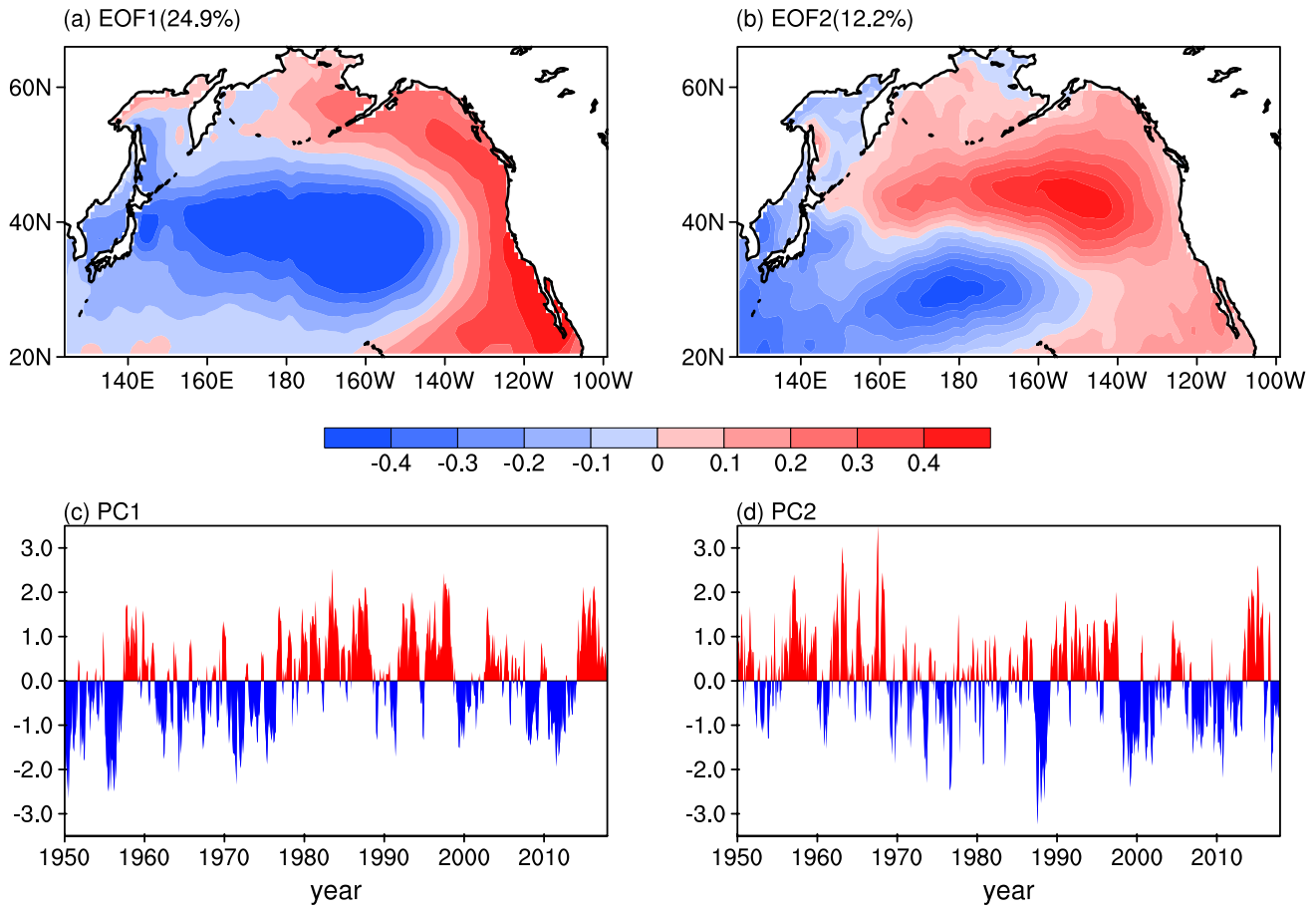

Fig. 1 Spatial patterns (**a**, **b**) and corresponding PCs (**c**, **d**) of the first two leading EOF modes of the North Pacific (20°–66° N, 124° E–99° W) monthly SSTA field (after removing the monthly mean global average SSTAs). Positive (red) and negative (blue) monthly values of the PC1 and PC2 time series are indicated by colored bars

EOF mode (EOF1) shows a structure typical of the Pacific Decadal Oscillation (Fig. 1a), and its time series (first principal component, PC1) has obvious interdecadal variations (Fig. 1c). The second EOF mode (EOF2, referred to as the VM) accounts for 12.2% of the total variance and exhibits a distinct dipole pattern over the extratropical North Pacific oriented in the northeast–southwest direction (Fig. 1b), in agreement with previous work (Bond et al. 2003; Ding et al. 2018, 2015b). The VM index is defined as the second principal component (PC2) associated with EOF2 (Fig. 1d). To describe the variation of the SNP SSTAs and WNP SSTAs related to the VM, the SNP_SST and WNP_SST indices are obtained by calculating the normalized SSTAs over the SNP (5°–25° N, 170°–110° W) and the WNP (10°–30° N, 110°–140°E) regressed on the VM index.

Several climate indices are also computed and analyzed in this work. The difference between the standardized SLP anomalies averaged over the northern (50°–69° N, 175°E–138° W) and southern (22°–40° N, 177°E–142° W) poles is known as the NPO index (Ding et al. 2015b). The Niño3.4 index, which is used to identify ENSO events, is defined by the SSTAs averaged over the region (5° S–5° N, 170°–120° W). These indices from 1950 to 2017 have all been linearly detrended and standardized using population standard deviations. In addition, to isolate the internal variability of the VM independent of ENSO, the effect of the previous winter's ENSO has been removed from the VM index using linear regression with respect to the Niño3.4 index. Since the SNP_SST and WNP_SST indices are defined based on the VM index, the effect of the previous winter's ENSO also has been removed from the SNP_SST and WNP_SST indices.

2.3 Methods

Correlation, linear regression, and composite analyses are also employed in this study. The statistical significance of these analyses was calculated using the two-tailed Student's *t*-test, in which the number of effective degrees of freedom N^* was calculated as described by Bretherton et al. (1999):

$$\frac{1}{N^*} \approx \frac{1}{N} + \frac{2}{N}\sum_{i=1}^{N}\frac{N-i}{N}R_X(i)R_Y(i),$$

where N is the number of available time steps and $R_X(i)$ and $R_Y(i)$ denote the autocorrelations of the two time series X and Y at lag time i, respectively.

3 Results

3.1 Relationship of the VM-related SNP-SSTA and WNP-SSTA with ENSO

To investigate the spatial structure of the VM and its linkage with atmospheric circulation variability, we present in Fig. 2 the SST, SLP and 10-m wind anomalies associated with the VM by regressing the North Pacific monthly SST, SLP and 10-m wind anomalies onto the VM index. The VM exhibits a tripole SSTA pattern over the entire North Pacific, including a tilted SSTA dipole structure oriented in the northeast–southwest direction over the North Pacific polewards of 20° N, along with a subtropical band of positive SSTAs extending from off the California coast to the central equatorial Pacific (Fig. 2a). The SSTA feature of the VM in the North Pacific bears some resemblance to the PMM-like (Chiang and Vimont 2004; Chang et al. 2007; Lin et al. 2015; Thomas and Vimont 2016; You and Furtado 2018) SSTA pattern, with a band of positive SSTAs over the SNP (Fig. 2a). Despite these similarities between the VM and PMM, there are notable differences between their SSTA patterns. One important difference in the SSTA pattern between the VM and PMM is the SSTA features over the WNP off the eastern coast of Asia. Therefore, while the two SST patterns are similar, the VM, as an SST mode covering the whole extratropical North Pacific basin, has its own characteristic SSTA pattern.

The SLPA pattern associated with the VM index exhibits a meridional dipole structure, characterized by a lobe of positive anomalies over the Aleutian Islands and broad negative SLPAs extending from 40° N to as far south as the equator (Fig. 2a). This result is generally consistent with previous findings that the VM is forced by an NPO-like atmospheric variability (Walker and Bliss 1932; Rogers 1981; Ding et al. 2015b). To illustrate the relationship between the NPO and VM, we calculated the lead–lag correlation between the monthly VM and NPO indices. The results showed that the correlation is highest when the NPO leads the VM by one month ($R = 0.45$, significant at the 99.9% confidence level), indicating an impact of the NPO on the VM (Fig. 2b). Additionally, the lead–lag correlations between the SNP_SST and WNP_SST and NPO indices closely resemble those between the VM and NPO indices, even though the peak correlation is relatively weaker than that between the VM and NPO indices (Fig. 2b).

The above results demonstrate that the spatial pattern of the VM covers the whole extratropical North Pacific basin, including the local-scale SSTAs over the SNP and WNP, which both arise from the NPO-like forcing. One may argue whether these local-scale SSTA patterns associated with the VM play different roles in the development of ENSO. To clarify this, we first examine the evolution of ENSO with respect to the SNP-SSTA and WNP-SSTA patterns, as represented by the lead–lag correlations between

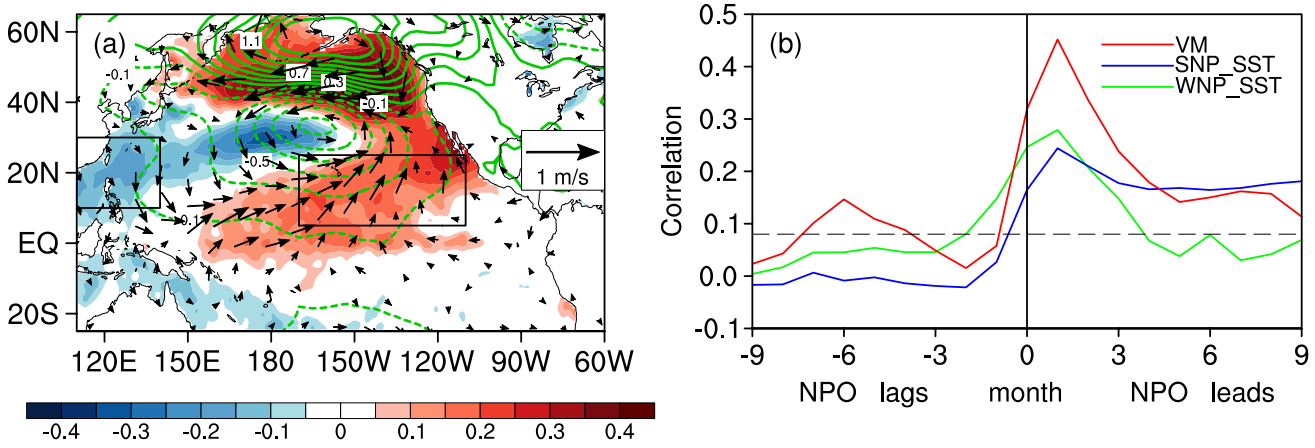

Fig. 2 **a** Regression maps of monthly SST (shaded; unit: °C), SLP (contours; unit: hPa) and 10-m wind anomalies (vectors; units: m s^{-1}) onto the monthly VM index. The contour interval is 0.2 hPa for SLPAs and the reference wind vector is 1 m s^{-1}. Only SST, SLP and 10-m wind anomalies significant at the 95% confidence level according to a two-tailed Student's t-test are shown. The two black boxes denote the locations of the subtropical northeast Pacific (5°–25° N, 170°–110° W) and the western North Pacific (10°–30° N, 110°–140° E), respectively. **b** Lead–lag correlation coefficients of the monthly VM, SNP_SST and WNP_SST with NPO indices. The horizontal dashed line indicates the 95% confidence level

the three-month running average Niño3.4 index and the February–April [FMA(0)]-averaged SNP_SST and WNP_SST indices (Fig. 3a). Hereafter, the year in which the VM peaks in FMA is expressed as year 0, and the preceding and subsequent years as year − 1 and + 1, respectively. The correlation between the SNP_SST and Niño3.4 indices peaks during December–February [DJF(+ 1)], lagging behind the peak of the VM during FMA(0) by about 10 months. Even though the peak correlation between the SNP_SST and Niño3.4 indices is weaker than that between the VM and Niño3.4 indices, the correlation is strong and significant (significant at the 99.9% confidence level) for lead times of several months from summer. In contrast, the correlation between the WNP_SST and Niño3.4 indices is much weaker than that between the VM and Niño3.4 indices and is no longer significant at the 99.9% confidence level from August to October [ASO(0)] to the following summer. These results indicate that the VM-related SNP-SSTA may be more closely linked to ENSO than is the VM-related WNP-SSTA.

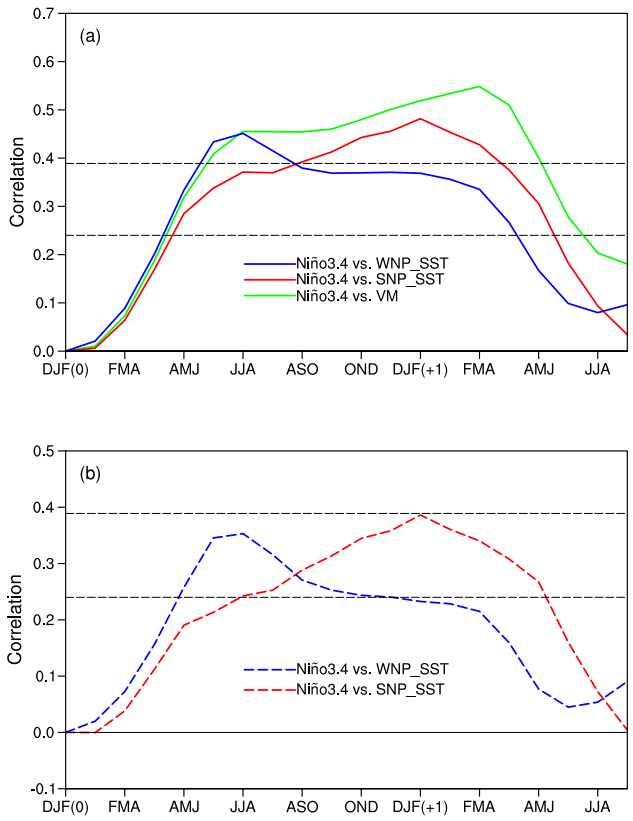

Fig. 3 **a** Lead–lag correlations of the FMA(0)-averaged VM, SNP_SST and WNP_SST indices with overlapping three-month average values of Niño3.4 index. **b** Lead–lag partial correlations of the FMA(0)-averaged SNP_SST and WNP_SST indices with overlapping three-month average values of Niño3.4 index calculated by linearly removing the FMA(0)-averaged WNP_SST and SNP_SST indices, respectively. In (**a**, **b**), the horizontal dashed lines show the 95% and 99.9% confidence level, respectively. The year in which ENSO develops is denoted as year (0), and the following year as year (+ 1)

3.2 Role of the VM-related SNP-SSTA and WNP-SSTA patterns in developing ENSO

To further focus in detail on the role of the SNP-SSTA and WNP-SSTA related to the VM in inducing the onset of ENSO, we examine the characteristics of the seasonal evolution of the SST and surface wind anomalies correlated with the FMA-averaged SNP_SST and WNP_SST indices (Fig. 4). During March–May (MAM), about one month after the peak of the VM, the SSTA pattern associated with the SNP_SST index in the SNP resembles the PMM-like pattern, with positive SSTAs extending from off the California coast to the central equatorial Pacific (Fig. 4a). Surface wind anomalies associated with the SNP_SST index result in convergence over the central equatorial Pacific, which in turn promotes the development of positive SSTAs in this region. These significant positive SSTAs in the central equatorial Pacific increase the zonal SSTA gradient along the western-central tropical Pacific via anomalous westerly winds in the western-central equatorial Pacific, which can effectively trigger a Bjerknes feedback that drives the development of an El Niño event during subsequent seasons. During DJF, an El Niño-like warming pattern is well developed in the central-eastern equatorial Pacific (Fig. 4g).

In contrast, for the WNP-SST, there is a significant VM-like SSTA pattern that is characterized by large loading over the WNP, along with a band of positive SSTAs in the mid-latitudes of the North Pacific and the SNP during MAM (Fig. 4b). The positive SSTAs in the SNP, combined with negative SSTAs in the WNP, lead to an increase in the zonal SSTA gradient across the western central tropical Pacific, which then induce the anomalous westerlies over the western central equatorial Pacific and thus a distinct conventional El Niño-like pattern during summer (Fig. 4d). However, due to the VM-related SSTAs in the WNP weakening in the following seasons, the zonal SSTA gradient associated with the WNP_SST index along the western–central tropical Pacific is smaller than that associated with the SNP_SST index from boreal fall to the following spring (Fig. 5a), which leads to weaker westerly wind anomalies in the western–central equatorial Pacific (Fig. 5b). This is insufficiently conducive to warming in the eastern equatorial Pacific owing to weaker westerly wind anomalies in the western–central equatorial Pacific associated with the WNP_SST index. As a result, during winter, the warming amplitude in the central-eastern equatorial Pacific associated with the WNP_SST index is smaller than that associated with the SNP_SST index (Fig. 4h). These results are consistent with the lead-lag correlations between the three-month running average Niño3.4

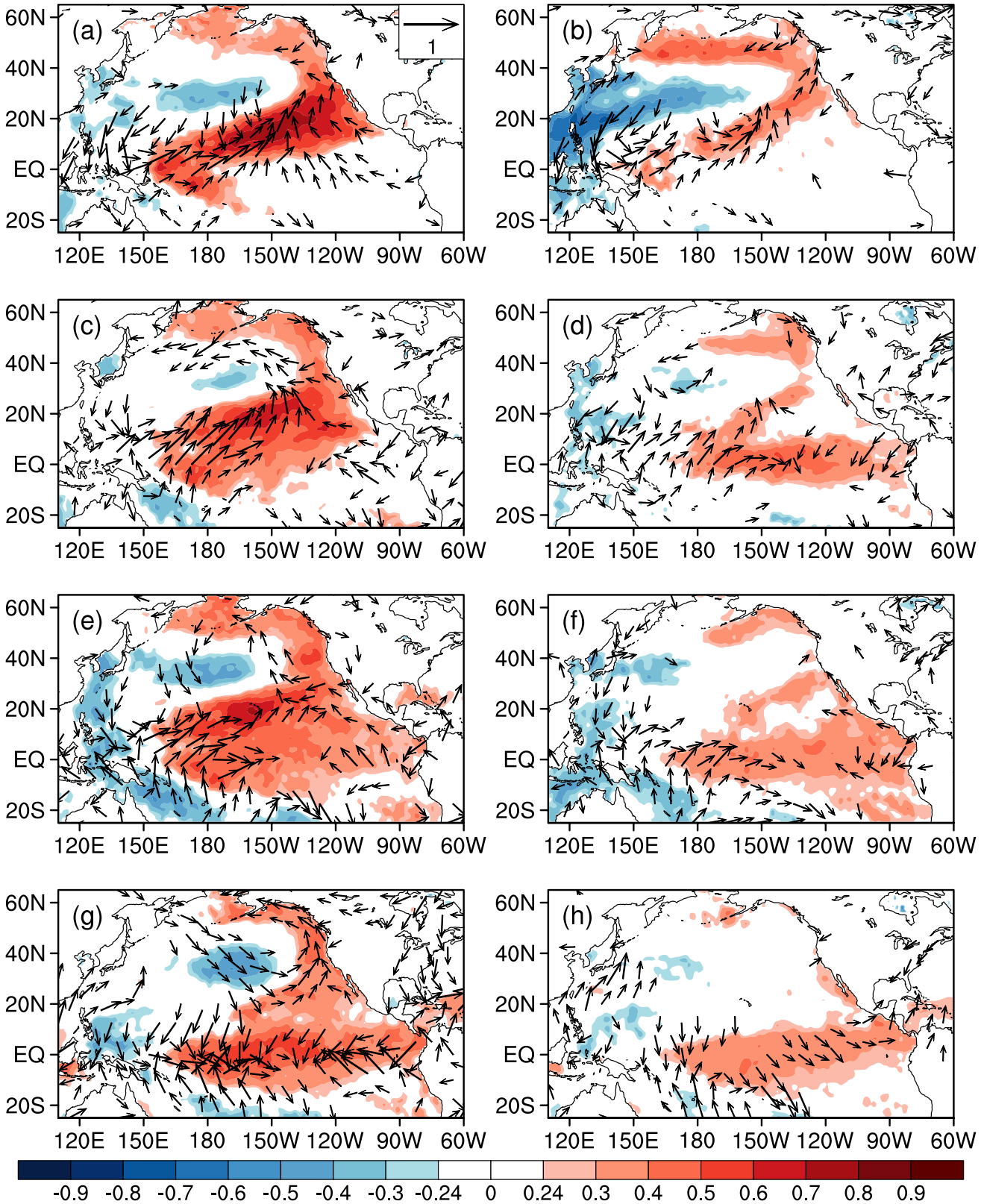

Fig. 4 Correlation maps of the three-month average SST (shaded) and surface wind (vectors) anomalies with the FMA(0)-averaged SNP_SST (left-hand panels) and inverted WNP_SST (right-hand panels) indices with the three-month average SST (shaded) and surface wind (vectors) anomalies for several lead times: **a**, **b** MAM(0), **c**, **d** JJA(0), **e**, **f** SON(0), and **g**, **h** DJF(+1). Positive (red) and negative (blue) SSTAs, with correlation significant at the 95% confidence level, are shaded. Only surface wind vectors significant at the 95% confidence level are shown

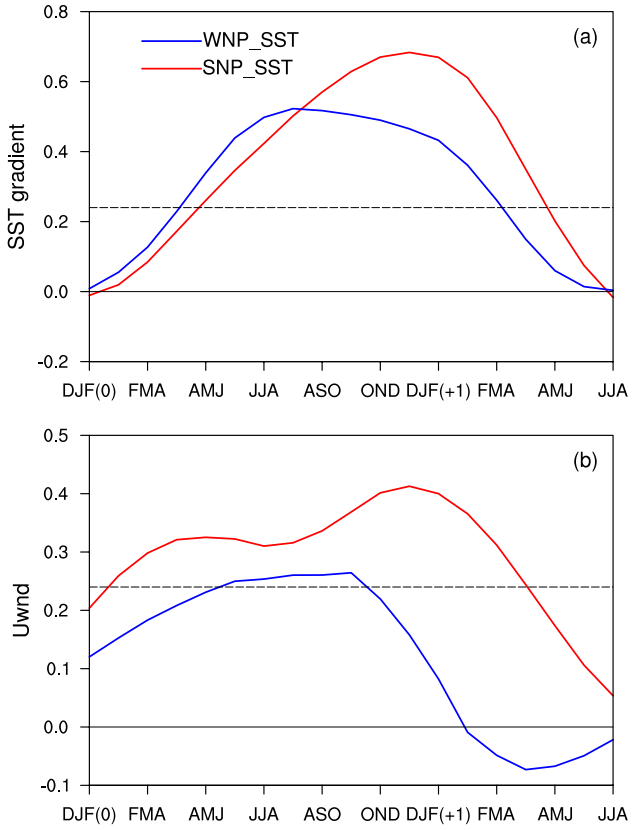

Fig. 5 **a** Lead–lag correlation coefficients of the SSTA gradient [defined as the difference between the 3-month running mean SSTAs over the western equatorial Pacific (5° S–5° N, 120°–150° E) and the three-month running mean SSTAs over the central equatorial Pacific (5° S–5° N, 180°–120° W)] with the FMA(0)-averaged SNP_SST and WNP_SST indices. **b** Lead–lag correlation coefficients of the three-month running mean surface zonal wind anomalies area-averaged over the western–central equatorial Pacific (5° S–5° N, 150° E–150° W) with the FMA-averaged SNP_SST and WNP_SST indices. In (**a**, **b**), the horizontal dashed lines show the 95% confidence level. The year in which ENSO develops is denoted as year (0), and the following year as year (+ 1)

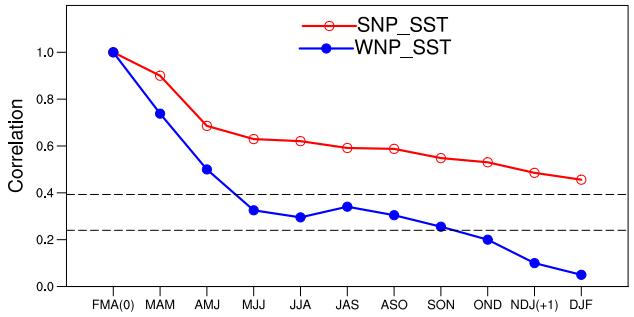

Fig. 6 The three-month lag autocorrelation curve of the SNP_SST (red line) and WNP_SST (blue line) indices based on a starting season of FMA(0). The horizontal dashed lines show the 95% and 99.9% confidence level

index and the FMA(0)-averaged SNP_SST and WNP_SST indices (Fig. 3a).

To further elucidate the cause of the different roles of these local-scale VM-related SSTAs in the tropical Pacific mentioned above, we investigate the temporal persistence of the VM-related SNP-SSTA and WNP-SSTA pattern by computing the 3-month lag autocorrelation of the SNP_SST and WNP_SST indices based on a starting season of FMA(0). Figure 6 shows that the autocorrelation of the VM-related SNP-SSTA pattern slightly reduces from spring to winter. By contrast, the autocorrelation of the VM-related WNP-SSTA pattern decays rapidly from MAM(0) and is much lower than that of the VM-related WNP-SSTA pattern from summer to winter. To quantify the difference in the temporal persistence between the VM-related SNP-SSTA and WNP-SSTA patterns, we examine the persistence time, which is defined as the time (i.e., lag) for the maximum correlation coefficient to decay to its 1/e value. As expected, the persistence times of the VM-related SNP-SSTA and WNP-SSTA patterns are 12 and 6 months, respectively. Physically, the VM-related SNP-SSTA evolves via a thermodynamic coupling, referred to as the wind–evaporation–SST (WES) feedback (Xie and Philander 1994). This positive feedback enhances the persistence of SSTAs in the SNP via the impact of anomalous wind speed on evaporation (Liu and Xie 1994; Martinez-Villalobos and Vimont 2017; Vimont 2010). As a result, the high persistence of the SNP-SSTA induces anomalous westerly winds in the western–central equatorial Pacific from summer to winter, which can effectively trigger the development of an El Niño event during winter. Different from the SNP-SSTA pattern, the evolution of the VM-related WNP-SSTA experiences an eastward shift and fading (Fig. 4). Therefore, the persistence of SSTAs in the WNP is much lower than that of SSTAs in the SNP. These results further suggest that these two local-scale SSTA patterns associated with the VM may play different roles in developing ENSO.

The results presented thus far indicate that positive SSTAs in the SNP associated with the VM became more capable of inducing westerly wind anomalies in the western–central equatorial Pacific and thus enhanced air–sea surface coupling over the subtropical/tropical Pacific, which eventually contribute to the development of ENSO events. The process by which the VM-related SNP-SSTA influences ENSO may correspond to the SFM, which emphasizes a process of atmosphere–ocean interaction (Vimont et al. 2001, 2003a, b). In contrast, due to the lower persistence of the negative SSTAs in the WNP associated with the VM from summer to winter, the WNP-SSTA is not conducive to an intensification of surface wind anomalies and thus air–sea surface coupling. This raises the question as to whether the VM-related WNP-SSTA pattern is tied to anomalous subsurface ocean temperatures in the tropical Pacific.

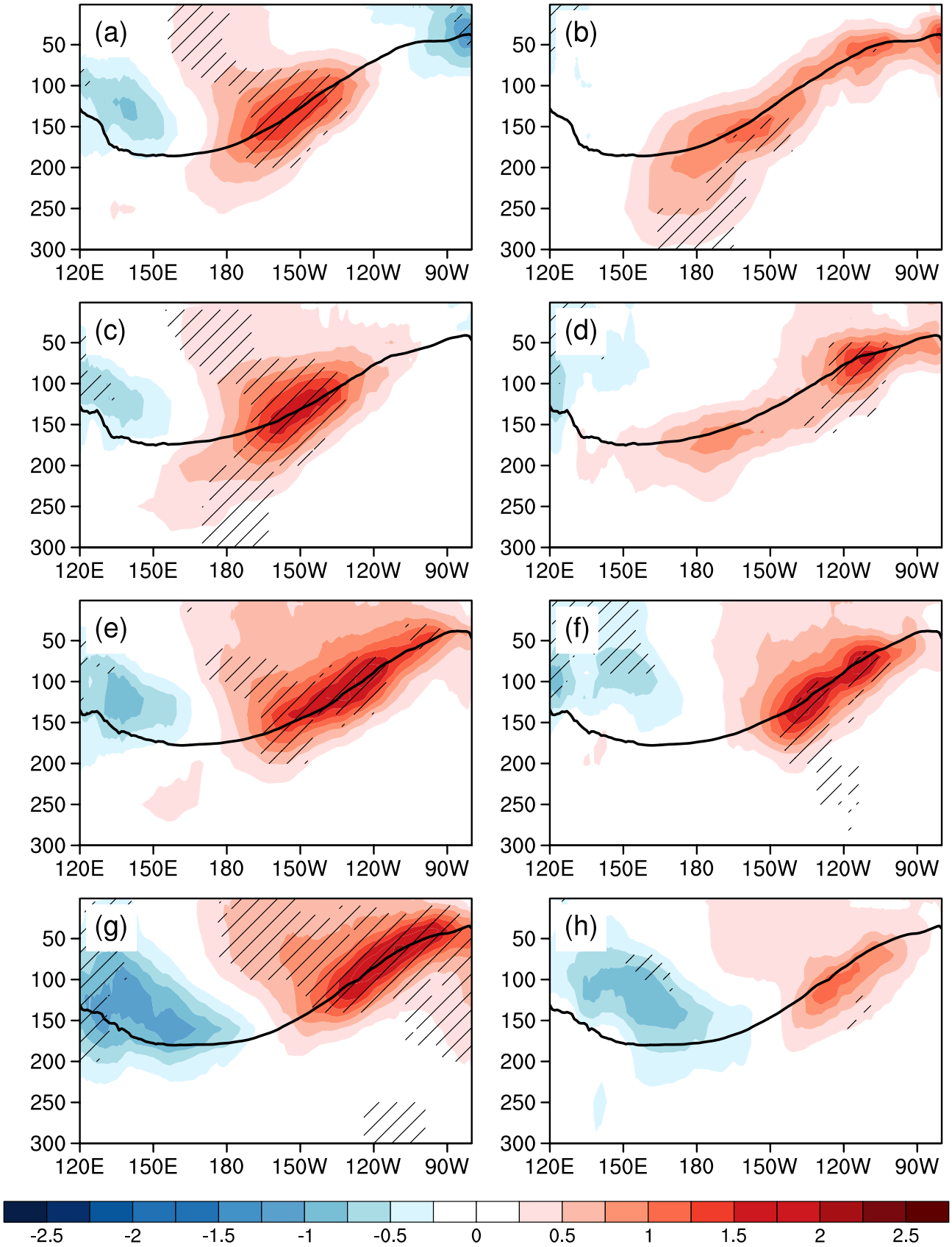
(a)
(b)
(c)
(d)
(e)
(f)
(g)
(h)
50
100
150
200
250
300
120E
150E
180
150W
120W
90W
-2.5
-2
-1.5
-1
-0.5
0
0.5
1
1.5
2
2.5

◂**Fig. 7** The composite difference in three-month average subsurface ocean temperature anomalies at various depths (unit: m) averaged over 5° S–5° N for several lead times: **a**, **b** MAM(0), **c**, **d** JJA(0), **e**, **f** SON(0), and **g**, **h** DJF(+1) between the positive and negative (left-hand panels) SNP_SST events and (right-hand panels) WNP_SST events, respectively. The oblique lines denote values that exceed the 95% confidence level

Accordingly, we next compare the seasonal evolution of subsurface temperature anomalies associated with the SNP_SST and WNP_SST indices averaged between 5° S and 5° N in the tropical Pacific (Fig. 7). We classify all of the SNP_SSTA and WNP_SSTA events into positive and negative SNP_SST (WNP_SST) events, which are defined as a year when the SNP_SST (WNP_SST) index is greater than one standard deviation and less than one negative standard deviation, respectively (Table 1). For the WNP-SST (right-hand panels in Fig. 7), significant positive subsurface ocean temperature anomalies occur in the western–central equatorial Pacific (between 150° E and 150° W) at depths of around 100–300 m during MAM, which appear to be stimulated by anomalous westerly winds in the western equatorial Pacific, which may drive downwelling equatorial Kelvin waves and induce a deepening of the thermocline in the western–central equatorial Pacific (Fig. 7b). After MAM, the positive subsurface temperature anomalies associated with the VM propagate upwards and eastwards along the thermocline and reach the eastern Pacific where they tend to strengthen the surface warming during SON (Fig. 7f). In contrast, for the SNP_SST events (left-hand panels in Fig. 7), significant positive subsurface temperature anomalies can be seen mainly in the central equatorial Pacific (between 180° and 120° W) at depths of around 50–200 m during MAM. At this time, negative subsurface temperature anomalies associated with the SNP_SST events occur in the eastern equatorial Pacific, which suppresses upward propagation of the positive subsurface temperature anomalies related to the SNP-SST (Fig. 7a). As a result, positive subsurface temperature anomalies associated with the SNP_SST events remain almost stationary, with only a slight eastward propagation during subsequent seasons, thereby limiting sea-surface warming in the central-eastern equatorial Pacific. These results are consistent with the seasonal evolution of the SSTAs associated with the FMA-averaged SNP_SST and WNP_SST indices mentioned above (Fig. 4).

To further examine the differences in the processes through which the VM-related SNP-SSTA and WNP-SSTA pattern affect ENSO, Fig. 8 shows the composite differences in the three-month running average thermocline depth (TCD; represented by the depth of the 20 °C isotherm) anomalies averaged over 5° S–5° N between the positive and negative SNP_SST (WNP_SST) events. For WNP_SST events (Fig. 8b), the significant positive TCD anomalies in the tropical Pacific are limited to between 120° E and 180° before spring [MAM(0)]. After spring, these positive TCD anomalies associated with the WNP-SST propagate eastwards along the equator and reach the eastern tropical Pacific in winter. Physically, the anomalous westerly winds could stimulate Kelvin waves on the oceanic TCD to eventually trigger the ENSO event (Wyrtki 1975; Kessler et al. 1995; Hendon et al. 1998; Clement et al. 2010). Therefore, these results indicate that the VM-related WNP-SSTA pattern is significantly linked to the variation in anomalous subsurface ocean temperatures in the tropical Pacific, which lends support to the finding that the SSTAs over the WNP contribute directly to oceanic Kelvin wave activity in the western tropical Pacific that precedes ENSO events (Wang et al. 2012). By contrast, tropical Pacific TCD anomalies related to the SNP_SST events show a dipole structure for lead times of up to a year, with positive TCD anomalies in the eastern tropical Pacific and negative TCD anomalies in the western tropical Pacific (Fig. 8a). It is noteworthy that the eastward propagation of the positive TCD anomalies in the equatorial Pacific is much weaker in this case, which indicates relatively weak subsurface ocean activity associated with the SNP-SSTA.

The above results verify that the negative SSTAs over the WNP associated with the VM tend to drive downwelling equatorial Kelvin waves in the western tropical Pacific induced by the variations in the North Pacific trade winds and cause the subsurface ocean temperature anomalies along the equator to propagate eastwards and upwards, thereby intensifying the warming in the central–eastern equatorial Pacific, which triggers the onset of ENSO via a thermocline–SST feedback process along the equator. Consequently, the influence on ENSO of the negative SSTAs in the WNP related to the VM may be consistent with the TWC mechanism, which underlines the variation in subsurface ocean temperature anomalies along the equator (Anderson 2003, 2004; Anderson and Maloney 2006; Anderson et al. 2013b).

Therefore, the VM-related SNP-SSTA and WNP-SSTA patterns do indeed have quite distinct dynamic processes, which play different roles in the development of ENSO. Taken together we may conclude that, as the VM combines the effect of SSTAs in the SNP and the WNP, the VM may influence the onset of ENSO through two dominant processes: a surface thermodynamic process associated with the SNP-SSTA, and a thermocline–SST feedback process along the equator related to the WNP-SSTA. Furthermore, these results are reminiscent of the previous finding that zonal advective feedback plays a key role in the development of central-Pacific (CP) ENSO events, while thermocline feedback is a crucial process with respect to eastern-Pacific (EP) ENSO events (Kug et al. 2009, 2010). Our results imply that the VM-related SNP-SSTA and WNP-SSTA may be conducive to affecting CP and EP ENSO events, respectively. Figure 9 shows the composite difference

Table 1 Classification of years in which positive or negative SNP_SST and WNP_SST events occurred during the period 1950–2017

Positive SNP_SST events	Negative SNP_SST events	Positive WNP_SST events	Negative WNP_SST events
1958, 1959, 1960, 1968, 1974, 1978, 1980, 1982, 1986, 1994, 2015, 2017	1964, 1965, 1971, 1983, 1987, 1992, 1998, 1999, 2000, 2008, 2011, 2012,	1951, 1962, 1963, 1968, 1971, 1977, 1992, 1995, 2011	1959, 1960, 1966, 1979, 1988, 1999, 2001, 2017

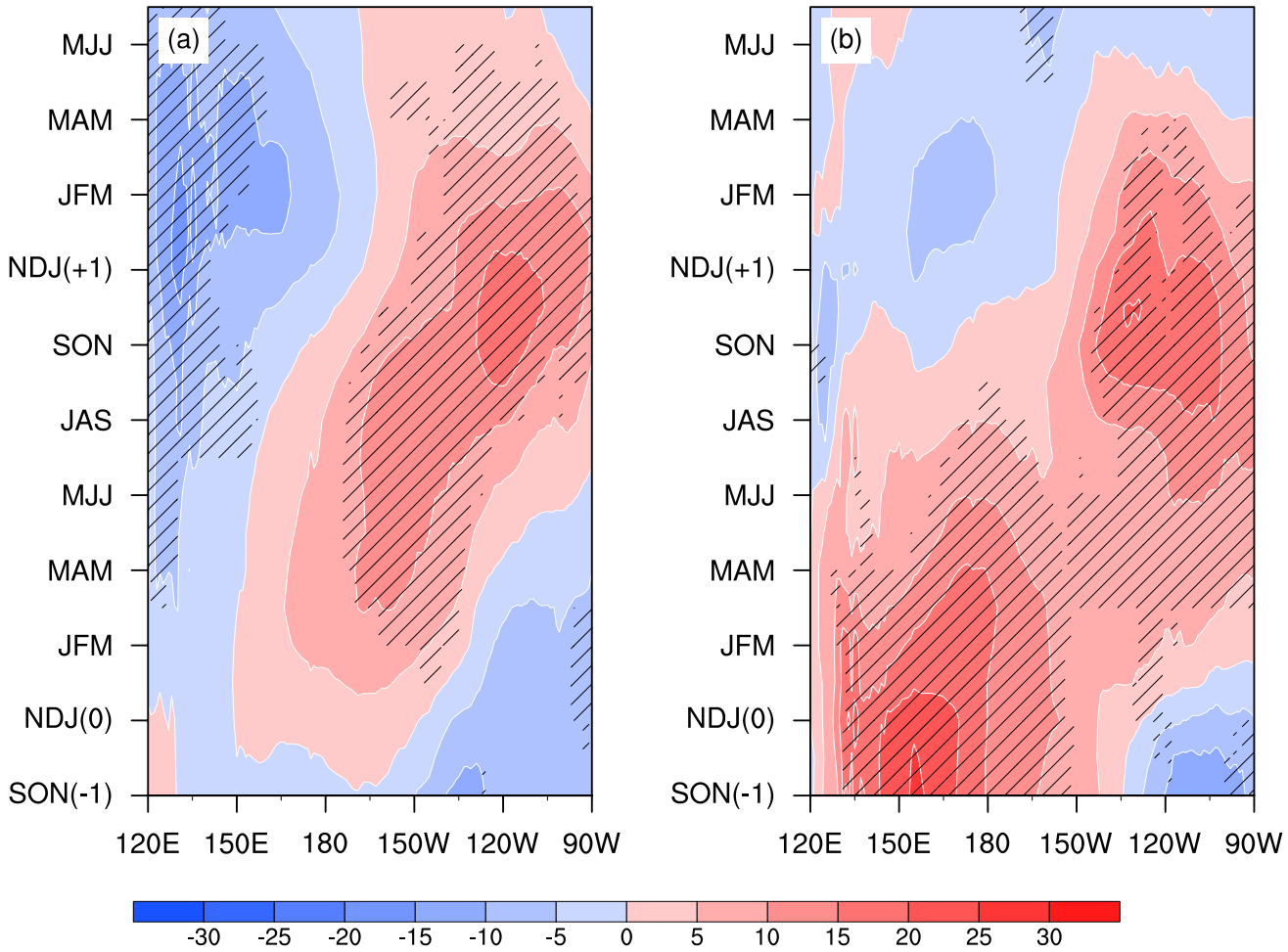

Fig. 8 Time–longitude cross-section of the composite difference in thermocline depth (approximated by the depth of the 20 °C isotherm) anomalies averaged over 5° S–5° N between the positive and negative **a** SNP_SST events and **b** WNP_SST events, respectively. The oblique lines denote values that exceed the 95% confidence level

in the SSTA averaged over 5° S–5° N between the positive and negative SNP_SST (WNP_SST) events. As expected, positive SSTAs related to the SNP_SST appear in the central tropical Pacific during the ENSO developing phase and peak in the Niño4 region (5° N–5° S, 160° E–150° W) during the mature phase of ENSO (Fig. 9a). As for WNP_SST, negative SSTAs over the eastern tropical Pacific experience an apparent phase transition to positive SSTAs in MAM(0) that intensify and propagate westwards along the equator during the following seasons. These positive SSTAs associated with the WNP_SST peak in the Niño3 region (5° N–5° S, 150°–90° W) in the following winter (Fig. 9b). Therefore, as the VM combines effects of the SNP-SSTA and WNP-SSTA patterns, it tends to be followed by a mixed pattern of CP and EP ENSO events (Ding et al. 2015b).

3.3 Relative independent contributions of the VM-related SFM and TWC mechanism in developing ENSO

The analyses presented above confirm the distinct roles of VM-related SFM and the TWC mechanism in the

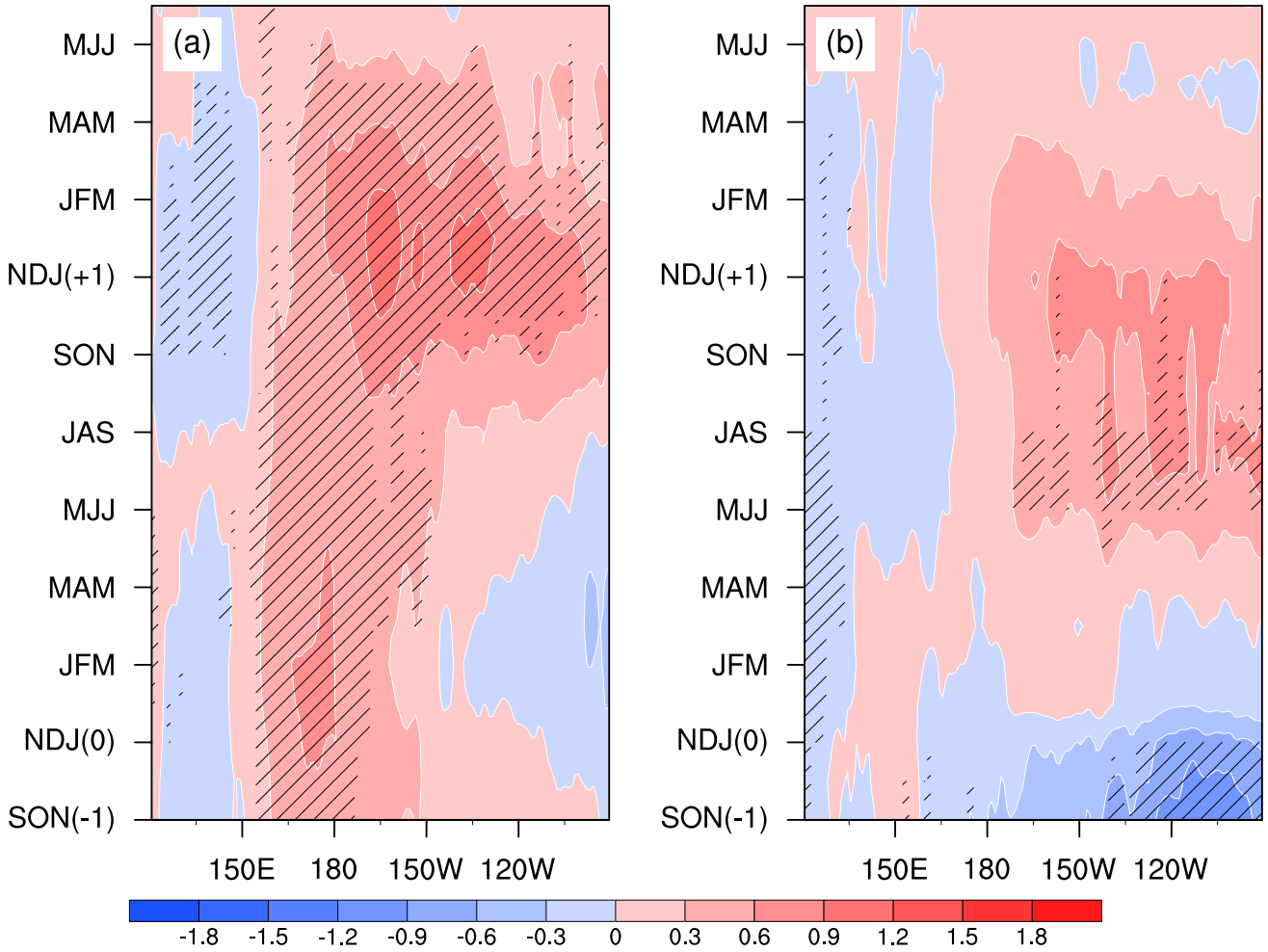

Fig. 9 As in Fig. 8 but for SSTAs

development of ENSO. Specifically, the SSTAs over the SNP and the WNP effectively trigger the initiation of ENSO via the SFM and the TWC mechanism, respectively. Further, to understand the relative contributions of the SNP-SSTA-related SFM and the WNP-SSTA-related TWC mechanism in the onset of ENSO, we first examine the relative independent relationships of the SFM and the TWC mechanism with the development of ENSO, as represented by the partial correlation between the FMA(0)-averaged SNP_SST (WNP_SST) index and the three-month running average Niño3.4 index by linearly removing the WNP_SST (SNP_SST) index shown in Fig. 3b. With the removal of the WNP_SST effect, the correlations between the SNP_SST and Niño3.4 indices are slightly reduced but still significant at or above the 95% confidence level for lead times of up to a year. In contrast, with the removal of the SNP_SST effect, the WNP_SST-related Niño3.4 index decays rapidly after reaching its peak during JJA(0) and does not persist through the following winter, suggesting that the WNP-SST tends to induce a faster phase transition of El Niño, thereby destroying favorable conditions for the development of El Niño events. These results indicate that the VM-related SNP-SSTA may play an independent role in affecting ENSO and the linkage between the VM-related WNP-SSTA and ENSO depends upon the presence of the SNP-SSTA.

As mentioned above, the VM-related SNP-SSTA is more closely linked to ENSO than is the VM-related WNP-SSTA, indicating that the SFM may be more conducive to inducing ENSO than the TWC mechanism. However, an important question is the relative independent contributions of these two mechanisms in ENSO. To address this, we examine the probabilities of ENSO events that are preceded by the VM-related SNP_SST and WNP_SST events, respectively. Figure 10 shows that the probability of an ENSO event being preceded by a VM-related SNP_SST or WNP_SST event is comparable (51.2% and 50.0%, respectively). However, the probability of an El Niño (La Niña) event being preceded by a positive (negative) VM-related SNP_SST or WNP_SST event is noticeably different. Specifically, it was found that positive (negative) SNP_SST events [36.7% (68.2%)] may

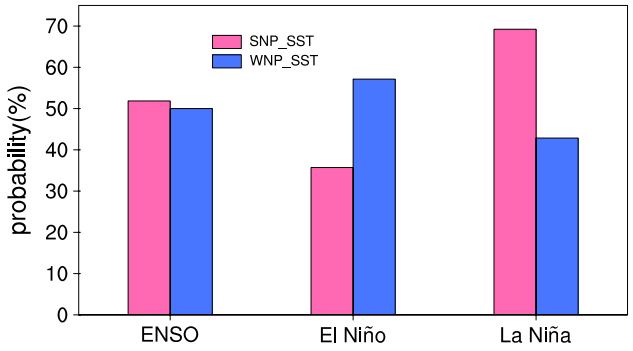

Fig. 10 The ratios of ENSO, El Niño and La Niña events when total, positive and negative SNP_SST (pink bar) and WNP_SST (blue bar) events occur during the FMA(0)

induce fewer El Niño events (more La Niña events) than positive (negative) WNP_SST events [57.4% (41.8%)]. Given that the evolution of the warm and cold phases of ENSO display prominent asymmetric features of the meridional position of SST (Yu 2011; Anderson et al. 2013a), this result is therefore consistent with the finding mentioned above that the VM-related SNP-SSTA and WNP-SSTA may be conducive to affecting CP and EP ENSO events, respectively.

To further verify the relative contributions of the SFM and the TWC mechanism associated with the VM in ENSO, we use the output of the first 30 members of the CESM-LENS from 1950 to 2005. First, we examine if the 30 members used in the present study can reproduce the spatial patterns of the VM. Figure 11 shows that most of the members of the CESM-LENS can reproduce the spatial patterns of the VM reasonably well. The pattern correlations between the observation and most of the members are higher than 0.75 (26 of 30 members). Thus, the SNP_SST and WNP_SST indices in the CESM-LENS models follow the same definitions as used for the observations.

The relative contributions of the SFM and the TWC mechanism associated with the VM in inducing ENSO events is also examined in the first 30 members of the CESM-LENS (1950–2005) simulations (Fig. 12). Among the 30 members, 18 show partial correlations between the FMA(0) SNP_SST and the DJF(+1) Niño3.4 indices that are higher than those between the FMA(0) WNP_SST and the DJF(+1) Niño3.4 indices, which indicates that nearly half of the members of the CESM-LENS underestimate the link between the VM-related SNP-SSTA and ENSO. However, further analysis of these 18 members of the CESM-LENS shows that 12 of them (> 60%) generate a lower (higher) occurrence ratio of El Niño (La Niña) being preceded by positive (negative) SNP_SST events than positive (negative) WNP_SST events (Fig. 12b, c). The multi-model ensemble result is consistent with the above analysis and further highlights the different roles played by the VM-related SNP-SSTA and WNP-SSTA in the development of ENSO. Therefore, even though the VM-related SFM may be more conducive to inducing ENSO than the TWC mechanism, these two mechanisms both play a crucial role in ENSO.

4 Summary and discussion

This paper has focused on a detailed investigation of the different roles and relative contributions of the SFM and TWC mechanism associated with the VM in ENSO. As mentioned above, the VM exhibits a basin-scale SST mode over the North Pacific, including positive SSTAs over the SNP and negative SSTAs over the WNP. Our results emphasize that local-scale SSTAs in both the SNP and the WNP are important components of the VM-related SSTA pattern in the North Pacific and play different roles in the development of ENSO. The VM-related SNP-SSTA evolves via WES feedback, which enhances the temporal persistence of SSTAs in the SNP. As a result, the high persistence of the SNP-SSTA induces anomalous westerly wind anomalies in the western–central equatorial Pacific from summer to winter, which can effectively trigger the development of an El Niño event during winter. In contrast to SSTAs in the SNP that may exert effects on ENSO primarily through thermodynamic coupling, SSTAs in the WNP tend to drive downwelling equatorial Kelvin waves in the western tropical Pacific induced by the variations in the North Pacific trade winds and cause the variation in the subsurface ocean temperature anomalies along the equator, which induce the development of ENSO via a thermocline–SST feedback process along the equator. Consequently, as the VM combines effects of SNP-SSTA and WNP-SSTA patterns, it may influence the onset of ENSO through two dominant processes: the SFM associated with the SNP-SSTA and the TWC mechanism associated with the WNP-SSTA, which is clearly illustrated schematically in Fig. 13.

Our results further reveal that the SNP-SSTA-related SFM may play an independent role in affecting ENSO and is more closely linked to ENSO than is the WNP-SSTA-related TWC mechanism. Given that the distinct role of SNP-SSTA and WNP-SSTA related to the VM playing in ENSO, furthermore, the relative contribution of the SFM and the TWC mechanism associated the VM in ENSO was examined. It was found that the SFM may induce fewer El Niño events

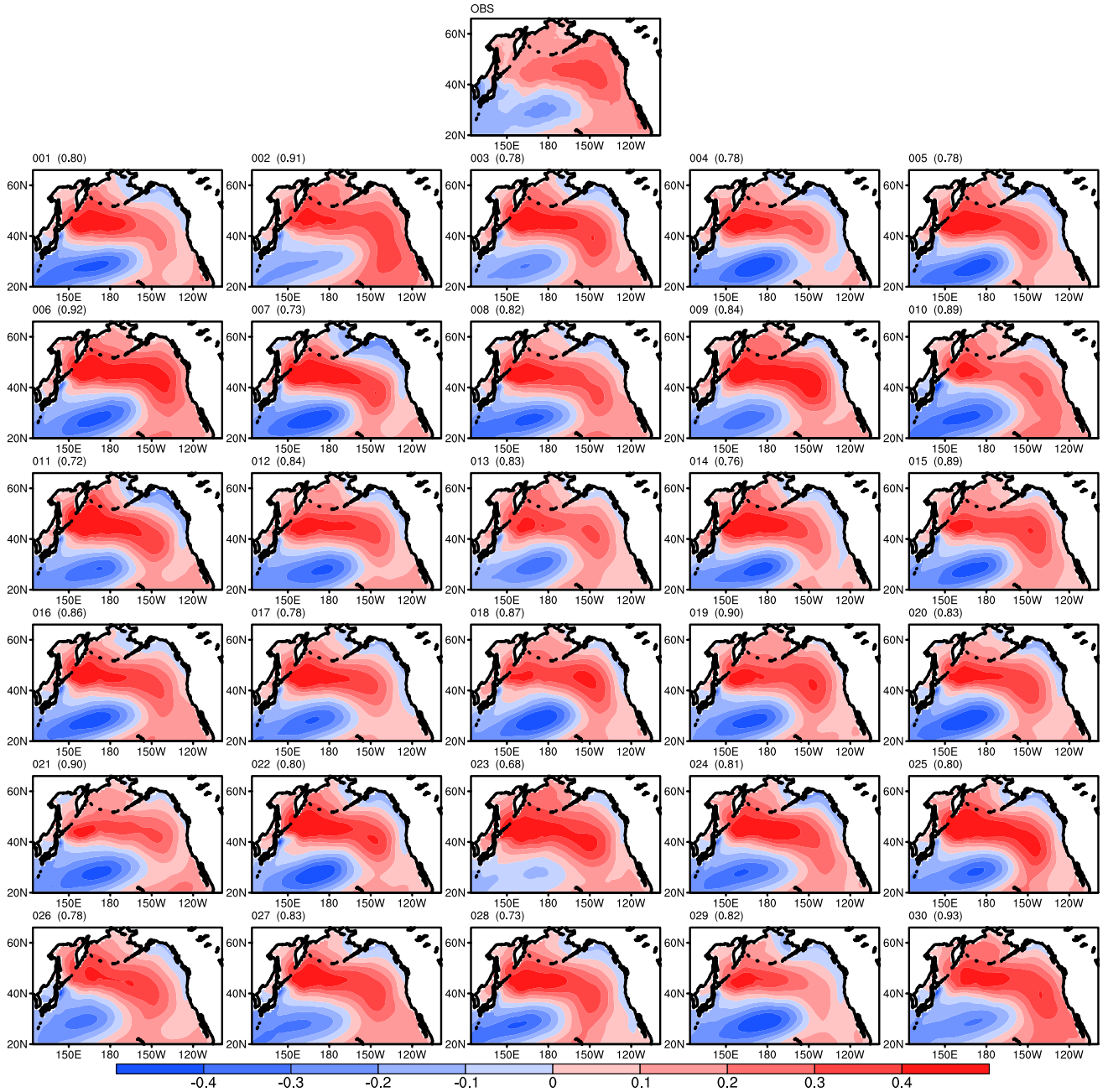

Fig. 11 Spatial patterns of the second EOF mode of the SSTAs over the North Pacific (20°–66° N, 124° E–99° W) calculated from observation (OBS) and 30 members of the CESM-LENS (001–030). The numbers in brackets in the upper-left corner of each panel indicate the pattern correlation between the observation and each member of the CESM-LENS

(more La Niña events) than the TWC mechanism, which is consistent with the finding that the VM-related SNP-SSTA and WNP-SSTA patterns may be conducive to affecting CP and EP ENSO events, respectively. These differences were supported in this study by using CESM-LENS outputs.

The present work has implications for understanding the distinct roles and the relative contributions of the SFM and TWC mechanism associated with the VM in triggering ENSO, and thus for improving the predictability of different types of ENSO. It should be pointed out that, although our results highlight the importance of these two mechanisms

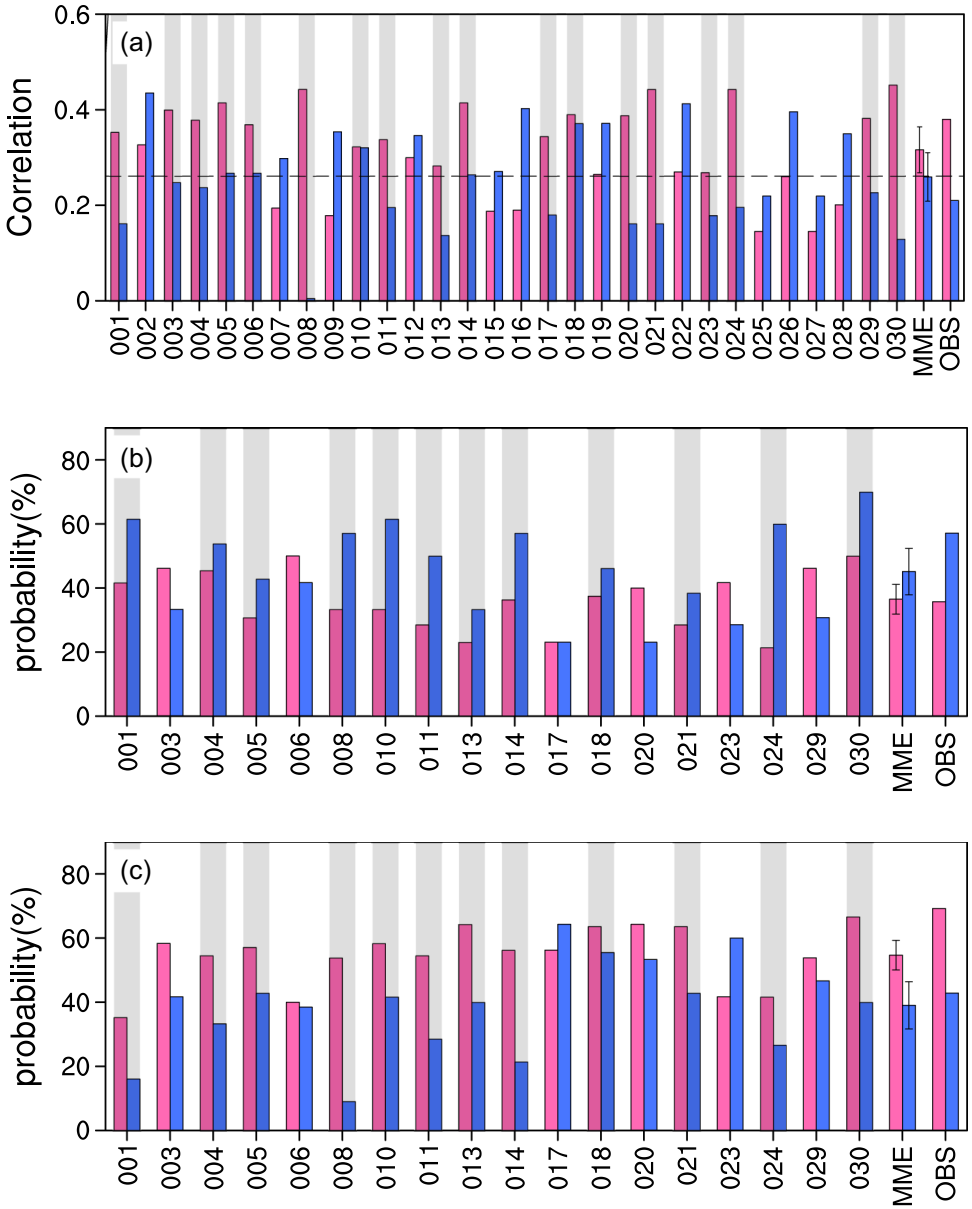

Fig. 12 **a** Partial correlations of the FMA(0)-averaged SNP_SST (pink bars) and WNP_SST (blue bars) indices with the DJF(+1) Niño3.4 index in the 30 members of the CESM-LENS calculated by linearly removing the FMA(0)-averaged WNP_SST and SNP_SST indices, respectively. Also shown is the multi-model ensemble (MME) mean of 30 members and observation (OBS). The horizontal dashed line shows the 95% confidence level. **b** Ratios of El Niño events when SNP_SST (pink bars) and WNP_SST (blue bars) events occur during the FMA(0) in the 18 members of the CESM-LENS. **c** As in (**b**) but for La Niña events. The error bars in the MME means indicate 0.5 standard deviations of inter-model variability. The gray shaded regions indicate that the results of the members are consistent with the observation

related to the VM in the initiation of ENSO, the results mainly focus on the linear linkage between the VM-related SSTA pattern and ENSO. However, the nonlinear effect of the VM-related SSTA pattern in tropical Pacific climate variability cannot be neglected. Further work is needed to quantify the relative contributions of the SFM and the TWC mechanism related to the VM in the development of different types of ENSO by conducting sensitivity experiments using a coupled general circulation model. In addition, further attention also needs to be paid to the mechanisms of interactions between low-frequency anomalies in the tropics and extratropics of the North Pacific (McCreary and Lu 1994; Gu and Philander 1997; Zhang and Levitus 1997; Zhang et al. 1998; Barnett et al. 1999; Kleeman et al. 1999; Liu et al. 2002).

Funding This work was jointly supported by the National Natural Science Foundation of China (41790474, 41975070).

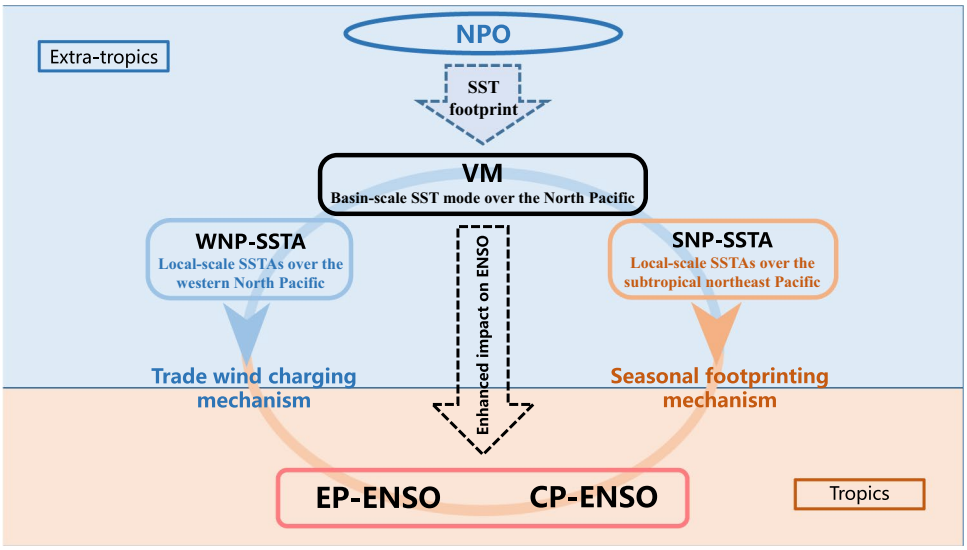

Fig. 13 Schematic diagram showing processes by which the VM-related SNP-SSTA and WNP-SST patterns influence the onset of ENSO. The VM-related SNP-SSTA pattern mainly influences the onset of CP ENSO via an air–sea surface thermodynamic coupling process over the subtropical/tropical Pacific (seasonal footprinting mechanism). In contrast, the VM-related WNP-SST pattern tends to affect the development of EP ENSO via a thermocline–SST feedback process along the equator (trade wind charging mechanism). As the VM combines the effects of the SNP-SSTA and WNP-SSTA patterns, as a basin-scale SST mode over the North Pacific, it may exert an enhanced impact on ENSO

Availability of data and material The Hadley Centre Global Sea Ice and Sea Surface Temperature data set are downloaded online (from https://www.metoffice.gov.uk/hadobs/hadisst/data/download.html). The National Centers for Environmental Prediction–National Center for Atmospheric Research Reanalysis data (Version I) are from the ESRL website (https://psl.noaa.gov/data/gridded/data.ncep.reanalysis2.pressure.html). The output of the Community Earth System Model Large Ensemble Community Project is available at https://www.cesm.ucar.edu/projects/community-projects/LENS/data-sets.html.

Declarations

Conflicts of interest/Competing interests The authors declare no conflicts of interest/competing interests.

Code availability The software application applied in the paper is the NCAR Command Language.

Ethics approval Not applicable.

Consent to participate The authors consent to participate.

Consent for publication The authors consent for publication.

References

Alexander MA, Bladé I, Newman M, Lanzante JR, Lau N-C, Scott JD (2002) The atmospheric bridge: the influence of ENSO teleconnections on air-sea interaction over the global oceans. J Clim 15:2205–2231

Anderson BT (2003) Tropical Pacific sea-surface temperatures and preceding sea level pressure anomalies in the subtropical North Pacific. J Geophys Res-Atmos 108:4732

Anderson BT (2004) Investigation of a large-scale mode of ocean-atmosphere variability and its relation to tropical pacific sea surface temperature anomalies. J Clim 17:4089–4098

Anderson BT, Maloney E (2006) Interannual Tropical Pacific Sea Surface Temperatures and Their Relation to Preceding Sea Level Pressures in the NCAR CCSM2. J Clim 19:998–1012

Anderson BT, Furtado JC, Cobb KM, Di Lorenzo E (2013a) Extratropical forcing of El Niño-Southern Oscillation asymmetry. Geophys Res Lett 40:4916–4921

Anderson BT, Perez RC, Karspeck A (2013b) Triggering of El Niño onset through trade wind–induced charging of the equatorial Pacific. Geophys Res Lett 40:1212–1216

Ashok K, Behera SK, Rao SA, Weng H, Yamagata T (2007) El Niño Modoki and its possible teleconnection. J Geophys Res Oceans 112:C11007

Barnett TP, Pierce DW, Latif M, Dommenget D, Saravanan R (1999) Interdecadal interactions between the tropics and midlatitudes in the Pacific basin. Geophys Res Lett 26:615–618

Bond NA, Overland JE, Spillane M, Stabeno P (2003) Recent shifts in the state of the North Pacific. Geophys Res Lett 30:2183

Bretherton CS, Widmann M, Dymnikov VP, Wallace JM, Bladé I (1999) The effective number of spatial degrees of freedom of a time-varying field. J Climate 12:1990–2009

Chakravorty S, Perez RC, Anderson BT, Larson SM, Giese BS, Pivotti V (2021) Ocean dynamics are key to extratropical forcing of El Niño. J Climate (published online ahead of print 2021). https://journals.ametsoc.org/view/journals/clim/aop/JCLI-D-20-0933.1/JCLI-D-20-0933.1.xml

Chang P, Zhang L, Saravanan R, Vimont DJ, Chiang JCH, Ji L, Seidel H, Tippett MK (2007) Pacific meridional mode and El Niño—Southern Oscillation. Geophys Res Lett 34:L16608

Cheng L, Trenberth KE, Fasullo J, Boyer T, Abraham J, Zhu J (2017) Improved estimates of ocean heat content from 1960 to 2015. Sci Adv 3:e1601545

Chiang JCH, Vimont DJ (2004) Analogous pacific and atlantic meridional modes of tropical atmosphere-ocean variability. J Clim 17:4143–4158

Clement AC, di Nezio PN, Deser C (2010) Rethinking the Ocean's Role in the Southern Oscillation. GC44A-03

Ding R, Li J, Tseng Y-H, Ruan C (2015a) Influence of the North Pacific Victoria mode on the Pacific ITCZ summer precipitation. J Geophys Res-Atmos 120:964–979

Ding R, Li J, Tseng Y-H, Sun C, Guo Y (2015b) The Victoria mode in the North Pacific linking extratropical sea level pressure variations to ENSO. J Geophys Res-Atmos 120:27–45

Ding R, Li J, Tseng Y-H, Li L, Sun C, Xie F (2018) Influences of the North Pacific Victoria Mode on the South China Sea Summer Monsoon. Atmosphere 9:229

Dou J, Wu Z, Zhou Y (2017) Potential impact of the May Southern Hemisphere annular mode on the Indian summer monsoon rainfall. Clim Dyn 49:1257–1269

Grimm AM, Tedeschi RG (2009) ENSO and extreme rainfall events in South America. J Clim 22(1589):1609

Gu D-F, Philander SGH (1997) Interdecadal climate fluctuations that depend on exchanges between the tropical and extratropics. Science 275:805–807

Hendon HH, Liebmann B, Glick JD (1998) Oceanic kelvin waves and the Madden-Julian oscillation. J Atmos Sci 55:88

Kalnay E, Kanamitsu M, Kistler R, Collins W, Deaven D, Gandin L, Iredell M, Saha S, White G, Woollen J, Zhu Y, Chelliah M, Ebisuzaki W, Higgins W, Janowiak J, Mo KC, Ropelewski C, Wang J, Leetmaa A, Reynolds R, Jenne R, Joseph D (1996) The NCEP/NCAR 40-year reanalysis project. Bull Am Meteorol Soc 77:437–472

Kao H-Y, Yu J-Y (2009) Contrasting Eastern-Pacific and Central-Pacific types of ENSO. J Clim 22:615–632

Kay JE, Deser C, Phillips A, Mai A, Hannay C, Strand G, Arblaster JM, Bates SC, Danabasoglu G, Edwards J, Holland M, Kushner P, Lamarque J-F, Lawrence D, Lindsay K, Middleton A, Munoz E, Neale R, Oleson K, Polvani L, Vertenstein M (2015) The Community Earth System Model (CESM) large ensemble project: a community resource for studying climate change in the presence of internal climate variability. Bull Am Meteorol Soc 96:1333

Kessler WS, McPhaden MJ, Weickmann KM (1995) Forcing of intraseasonal Kelvin waves in the equatorial Pacific. J Geophys Res 100:10613

Kleeman R, McCreary JP, Klinger BA (1999) A mechanism for generating ENSO decadal variability. Geophys Res Lett 26:1743–1746

Kug J-S, Jin F-F, An S-I (2009) Two types of El Niño events: cold tongue El Niño and warm Pool El Niño. J Climate 22:1499–1515

Kug J-S, Choi J, An S-I, Jin F-F, Wittenberg AT (2010) Warm pool and cold tongue El Ni?o events as simulated by the GFDL 2.1 coupled GCM. J Clim 23:1226–1239

Lin C-Y, Yu J-Y, Hsu H-H (2015) CMIP5 model simulations of the Pacific meridional mode and its connection to the two types of ENSO. Int J Climatol 35:2352–2358

Linkin ME, Nigam S (2008) The North Pacific oscillation west pacific teleconnection pattern: mature-phase structure and winter impacts. J Clim 21:1979

Liu Z, Xie S (1994) Equatorward propagation of coupled air-sea disturbances with application to the annual cycle of the Eastern Tropical Pacific. J Atmos Sci 51:3807

Liu Z, Wu L, Gallimore R, Jacob G (2002) Search for the origins of Pacific decadal climate variability. Geophys Res Lett 29:1404

Martinez-Villalobos C, Vimont DJ (2017) An Analytical Framework for Understanding Tropical Meridional Modes. J Climate 30:3303

McCreary JP, Lu P (1994) Interaction between the subtropical and equatorial ocean circulations: the subtropical cell. J Phys Oceanogr 24:466–497

Paek H, Yu J-Y, Qian C (2017) Why were the 2015/2016 and 1997/1998 extreme El Niños different? Geophys Res Lett 44:1848–1856

Rayner NA, Parker DE, Horton EB, Folland CK, Alexander LV, Rowell DP, Kent EC, Kaplan A (2003) Global analyses of sea surface temperature, sea ice, and night marine air temperature since the late nineteenth century. J Geophys Res-Atmos 108

Rogers JC (1981) The North Pacific oscillation. J Climatol 1:39–57

Santoso A, McPhaden MJ, Cai W (2017) The defining characteristics of ENSO extremes and the strong 2015/2016 El Niño. Rev Geophys 55:1079–1129

Santoso A, Hendon H, Watkins A, Power S, Dommenget D, England MH, Frankcombe L, Holbrook NJ, Holmes R, Hope P, Lim E-P, Luo J-J, McGregor S, Neske S, Nguyen H, Pepler A, Rashid H, Gupta AS, Taschetto AS, Wang G, Abellán E, Sullivan A, Huguenin MF, Gamble F, Delage F (2019) Dynamics and predictability of El Niño-Southern oscillation: an australian perspective on progress and challenges. Bull Am Meteorol Soc 100:403

Schubert SD, Chang Y, Suarez MJ, Pegion PJ (2008) ENSO and wintertime extreme precipitation events over the contiguous United States. J Climate 21:22–39

Thomas EE, Vimont DJ (2016) Modeling the mechanisms of linear and nonlinear ENSO responses to the Pacific meridional mode. J Climate 29:8745–8761

Vimont D (2010) Transient growth of thermodynamically coupled variations in the tropics under an equatorially symmetric mean state. J Clim 23:5771

Vimont DJ, Battisti DS, Hirst AC (2001) Footprinting: a seasonal connection between the tropics and mid-latitudes. Geophys Res Lett 28:3923–3926

Vimont DJ, Battisti DS, Hirst AC (2003a) The seasonal footprinting mechanism in the CSIRO general circulation models. J Clim 16:2653–2667

Vimont DJ, Wallace JM, Battisti DS (2003b) The seasonal footprinting mechanism in the Pacific: implications for ENSO. J Clim 16:2668–2675

Walker GT, Bliss EW (1932) World weather V. Mem r Meteorol Soc 4:53–84

Wang B, Wu R, Fu X (2000) Pacific-East Asian teleconnection: how does ENSO affect East Asian Climate? J Clim 13:1517–1536

Wang S-Y, L'Heureux M, Chia H-H (2012) ENSO prediction one year in advance using western North Pacific sea surface temperatures. Geophys Res Lett 39:L05702

Wu Z, Zhang P (2015) Interdecadal variability of the mega-ENSO–NAO synchronization in winter. Clim Dyn 45:1117–1128

Wyrtki K (1975) El Niño—the dynamic response of the equatorial Pacific Ocean to atmospheric forcing. J Phys Oceanogr 5:572

Xie S-P, Philander SGH (1994) A coupled ocean-atmosphere model of relevance to the ITCZ in the eastern Pacific. Tellus A 46:340–350

You Y, Furtado JC (2018) The South Pacific meridional mode and its role in tropical pacific climate variability. J Clim 31:10141–10163

Yu J-Y (2011) Reversed spatial asymmetries between El Niño and La Niña and their linkage to decadal ENSO modulation in CMIP3 models. J Clim 24:5423–5434

Yu J-Y, Kim ST (2010) Relationships between extratropical sea level pressure variations and the Central Pacific and Eastern Pacific types of ENSO. J Clim 24:708–720

Yu B, Lin H, Wu Z, Merryfield WJ (2018) The Asian-bering-North American teleconnection: seasonality, maintenance, and climate impact on North America. Clim Dyn 50:2023–2038

Zhang R-H, Levitus S (1997) Structure and cycle of decadal variability of upper ocean temperature in the North Pacific. J Clim 10:710–727

Zhang R-H, Rothstein LM, Busalacchi AJ (1998) Origin of upper-ocean warming and El Nino change on decadal time scales in the Tropical Pacific Ocean. Nature 391:879–883

Zhang P, Wu Z, Chen H (2017) Interdecadal variability of the ENSO-North Pacific atmospheric circulation in winter. Atmos Ocean 55(2):110–120

Zhang XC, Zhong S, Wu Z, Li Y (2018) Seasonal prediction of the typhoon genesis frequency over the Western North Pacific with a Poisson regression model. Clim Dyn 51(11):4585–4600

Zhang P, Wang B, Wu Z (2019) Weak El Niño and Winter Climate in the mid-high latitude Eurasia. J Clim 32:402–421